


Acoustic Subwavelength Manipulation of Particles with a Quasiperiodic Plate

Yang Wang¹,[✉] Licheng Luo,¹ Manzhu Ke,^{1,*} and Zhengyou Liu^{1,2}

¹Key Laboratory of Artificial Micro- and Nano-structures of Ministry of Education and School of Physics and Technology, Wuhan University, Wuhan 430072, China

²Institute for Advanced Studies, Wuhan University, Wuhan 430072, China

 (Received 28 October 2021; revised 6 December 2021; accepted 7 December 2021; published 21 January 2022)

Acoustic manipulation has been a topic of significant research in recent years. However, the trapping scale in the radiative acoustic field domain is severely limited by the diffraction limit of the classic wave. Here, we report on a simple strategy to create multiple acoustic diffraction-limit-broken spots at different spatial positions in the far-field region for a wide frequency range. The subwavelength acoustic field comes from the interference of the plentiful diffractive beams specific to a quasiperiodic structure plate. We analyze the acoustic radiation force of the gradient field at multiheight plane above the plate for different frequencies and further demonstrate acoustic pushing and ring-shaped trapping of polystyrene particles within this subwavelength region. This work could be envisaged to pave a way for high-resolution manipulation of tiny particles in biomedical and cell research fields.

DOI: [10.1103/PhysRevApplied.17.014026](https://doi.org/10.1103/PhysRevApplied.17.014026)

I. INTRODUCTION

Dexterous manipulation of microparticles, cells, and organisms in a noninvasive manner has been attracting great interest for research realms in optical physics, acoustic physics, chemistry [1], and biology [2]. Acoustic tweezers, as an emerging and versatile contactless manipulation technique, which handles particles based on the momentum transfer of acoustic field and acoustic radiation force (ARF), have been developed into a tool for various practical applications [3–6]. To date, theoretical design methods [7–10] and experimental technologies [11–36] on particle manipulation by ARF have gained rapid progress, and various mature platforms have emerged to realize feasible and precise acoustic contactless manipulation. For instance, acoustic trapping [11–20], levitation [21–28], patterning [29–33], and sorting [34–36] have been accomplished with the help of transducer or transducer arrays [15–18,25–31], or by use of surface acoustic waves produced by interdigital transducer devices [34,35], or with the artificially engineered acoustic fields generated by a phononic crystal plate and acoustic metamaterial [19–22,33,36]. However, the trapping scale in the radiative acoustic field domain is severely limited by the Rayleigh diffraction limit of the classic wave. It is not easy to obtain an ultrasmall region of subwavelength dimension, which still guarantees the ARF for particle manipulation.

Seeking new methods for particle manipulation within the subwavelength region is a pending challenge. The

reported work involving the subwavelength acoustic field manipulation of particles was realized either by the use of nonradiative acoustic evanescent wave-based forces in an acoustic near-field region [37] or by the resonant shell mode near the surface of the shell structure [38] or by the use of superoscillation acoustic wave packets generated by a specially designed complex acoustic mask [39]. Here, we propose a relatively simple strategy to create multiple acoustic diffraction-limit-broken spots at different spatial positions in the far-field region. By numerically and experimentally analyzing the feature of the acoustic fields and their ARF effect on particles, we conclude that this ultrasmall subwavelength acoustic field ensures ARF on small particles. Therefore, we further give a direct demonstration of acoustic pushing and trapping of polystyrene microparticles within this subwavelength region.

II. METHODS

A. Generation of the subwavelength acoustic field

Figure 1 shows the top view of the fabricated sample, which consists of a $150 \times 150 \text{ mm}^2$ steel plate penetrated with an eightfold quasiperiodic array of holes. The geometrical parameters are chosen as thickness $t = 1 \text{ mm}$ and the radius of the holes $r = 0.6 \text{ mm}$. To give a more intuitive illustration of the structural characteristics, an enlarged view of the central area of the plate is plotted in company. The diagram shows that the lattice is composed of two different basic units, square and rhombus (with holes at the vertices) with equal length of the side $a = 3 \text{ mm}$ and the vertex angle of rhombus is 45° .

*mzke@whu.edu.cn

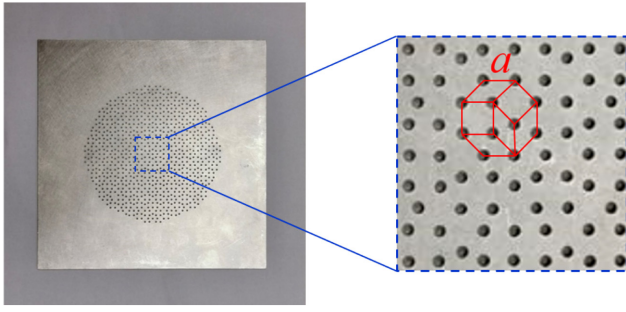


FIG. 1. Photograph of the fabricated sample perforated with an eightfold quasiperiodic array of holes. Inset: enlargement of the region marked by the blue dotted rectangle.

To characterize the performances of the acoustic fields generated by the proposed structure, we present the intensity profiles in the x - y plane at different spatial positions for different frequencies by means of numerical simulations and experimental measurements. Numerical modeling is performed by COMSOL Multiphysics, which is a finite-element analysis and solver software package. The material parameters used are listed below: $\rho = 7670 \text{ kg/m}^3$, $c_l = 6010 \text{ m/s}$, $c_t = 3230 \text{ m/s}$ for steel, $\rho = 1000 \text{ kg/m}^3$, $c_l = 1500 \text{ m/s}$ for water, and the symbols ρ , c_l , and c_t represent density, longitudinal, and transversal velocities, respectively. To verify the simulation results, an ultrasonic scanning device [40] (Panametrics LSC-02) is introduced to conduct the experimental measurement. In the experiment, a piezoelectric ultrasonic immersion transducer with a central frequency of 0.5 MHz (with an efficient working range of 0.25–0.75 MHz) is placed far away from the sample in the bottom of the water tank serving as the Gaussian-beam incidence source. The steel plate is fixed above the source by a specimen holder, and a receiving pinducer with a diameter of 1.2 mm is used to scan the acoustic field with a step length of 0.1 mm.

Figures 2(a1) and 2(a2) depict the simulated and measured intensity profiles in the field of view ($1.5\lambda \times 1.5\lambda$) at a vertical height $h = 3 \text{ mm}$ above the plate for frequency of 0.74 MHz (the corresponding wavelength λ is 2.03 mm), respectively. In the center of the figure, a small spot with a distinct gradient field distribution appears in the subwavelength region. To evaluate the spot more quantitatively, we redraw the simulation (black solid line) and measurement (red dotted line with circles) intensity data along the x axis (at $y = 0$), as shown in Fig. 2(a3), with the full width at half maximum marked (the dashed line in the figure). Apparently, the result manifests excellent performance of this design for generating the diffraction-limit-broken spot (about 0.42λ for 0.74 MHz). The ultrasmall region of subwavelength dimension is our expected manipulation goal. To show more possibilities, we change the working frequency and the x - y plane with different positions. Figures

2(b1)–2(b3) and 2(c1)–2(c3) illustrate results of the intensity distribution at $h = 3 \text{ mm}$ and $h = 6 \text{ mm}$ for 0.66 MHz (the corresponding wavelength λ is 2.28 mm), and the spots are approximately 0.36λ and 0.39λ , respectively.

To show more information about the subwavelength spots with our quasistructure plate in a larger region, we simulate the intensity field distributions in the y - z plane for frequency of 0.74 and 0.66 MHz, as shown in Figs. 3(a) and 3(b). Obviously, the results reveal that the subwavelength spots can be generated at multiple different spatial positions in the z direction. Here, we point out that the subwavelength spots do not come from the evanescent components of waves but the propagating waves. For a structure thin plate with a quasiperiodic array of holes, the diffractive components are plentiful and complex, which are induced by the long-range order of the quasistructure itself [41]. The delicate interference of the multiple different diffractive waves coming from the apertures generates subwavelength spots at the far field. Theoretically, for an infinite large plate, the subwavelength acoustic spots will reappear at different planes in the far field from the structure plate because the different diffractive waves can propagate far away and their interference field will reconstruct in the diffraction space. While for a plate with finite size and the limited acoustic wave source size and unavoidable loss of the wave in the propagation, the spot with subwavelength is always limited. As we show in Fig. 3, we see the spot construction effect but with an obvious dissipation.

B. Analysis of acoustic radiation force

According to the Gor'kov potential theory [42], small sphere particles of radius $r_p \ll \lambda$ (λ the wavelength of the acoustic field) will experience ARF due to the spatial gradient of acoustic intensity. The expression of ARF is given by

$$F^{\text{rad}} = -\nabla U^{\text{rad}}, \quad (1)$$

where U^{rad} stands for the force potential energy field.

$$U^{\text{rad}} = \frac{4\pi r_p^3}{3} \left[\frac{f_1}{2} \kappa_f \langle p_1 \rangle^2 - \frac{3}{4} f_2 \rho_f \langle v_1 \rangle^2 \right], \quad (2)$$

$f_1 = 1 - \kappa_p / \kappa_f$, $f_2 = 2(\rho_p - \rho_f) / (2\rho_p + \rho_f)$, where the angle brackets stand for time averaging, p_1 and v_1 represent the first-order pressure and velocity fields on the surface of the particle. The coefficients f_1 and f_2 are related to the compressibility and density of the fluid and particles, with subscripts f and p denoting fluid and particles, respectively. To show the particle-manipulation possibility of this subwavelength field, we investigate the dependence of ARF on the position of the polystyrene particle (density $\rho_p = 1050 \text{ kg/m}^3$, longitudinal velocity $c_p = 2350 \text{ m/s}$, mean radius $r_p = 90 \text{ }\mu\text{m}$) in the following.

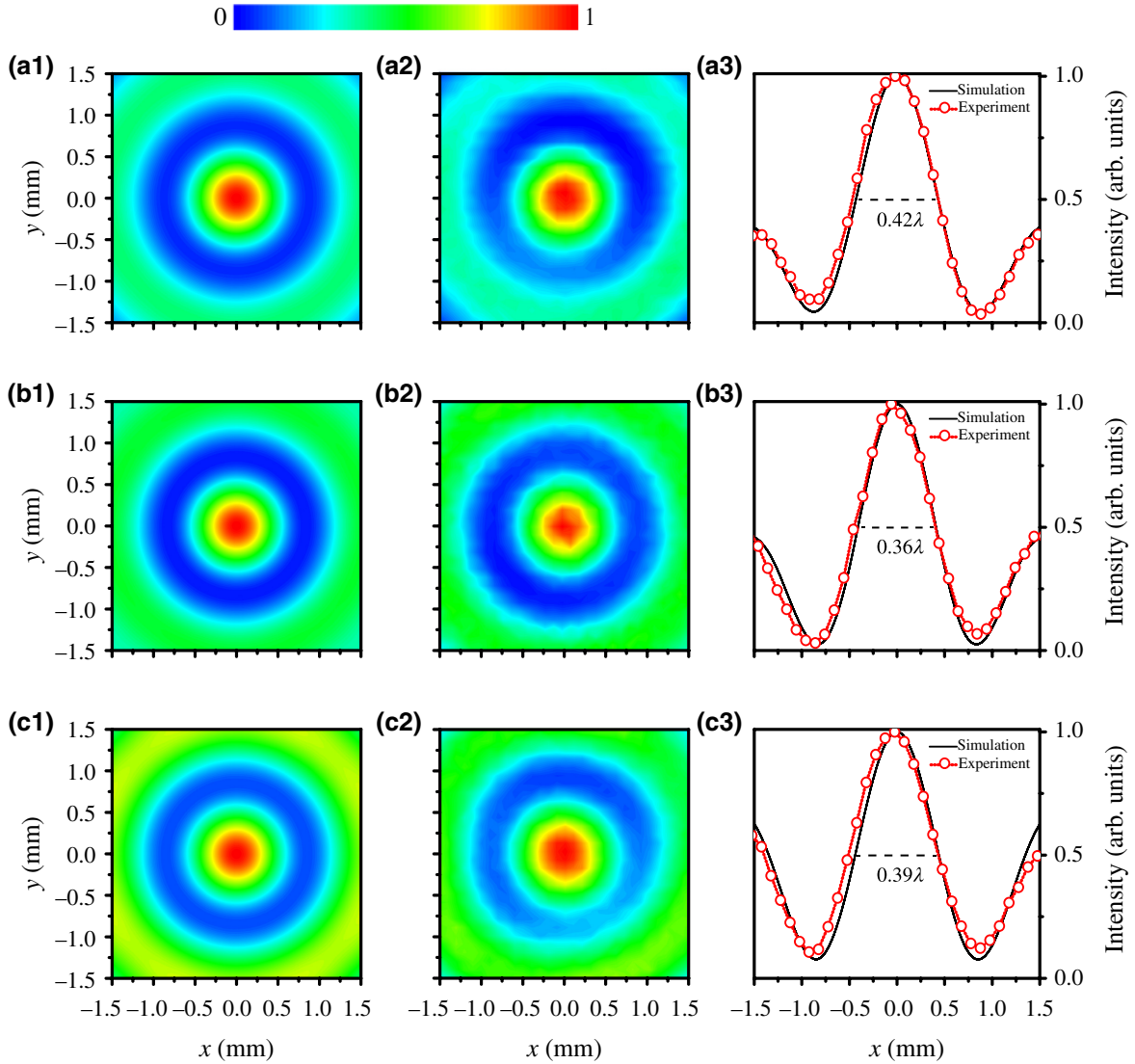


FIG. 2. (a1) and (a2) Simulated and measured intensity field distributions in the x - y plane at $h = 3$ mm for frequency of 0.74 MHz. (a3) The simulated and measured intensity distributions along the x axis (at $y = 0$), with the full width at half maximum marked (dashed line). (b1)–(b3), (c1)–(c3) The field distributions with frequency of 0.66 MHz at $h = 3$ mm and $h = 6$ mm, respectively.

Figure 4(a1) shows the calculated ARF distribution along the x - y plane at $h = 3$ mm with the frequency of 0.74 MHz, where the length and orientation of the arrows denote the magnitude and direction of the ARF, respectively. To confirm the numerical result, we present the experimental ARF distribution [Fig. 4(a2)] by substituting measured acoustic pressure data of the target plane into Eq. (1). Both the results reveal that particles will experience an attractive ARF directed to the first blue ring district, which corresponds to the potential well of the gradient field. To clearly show the stable position of the particles, we extract the simulated (black solid line) and measured (red dotted line with circles) result of ARF along the horizontal line at $y = 0$ [Fig. 4(a3)]. Here, we

define the positive or negative ARF according to the force vectors pointing right or left. Obviously, there are three zero-value points of ARF within this region. The first and the third zero-value points locating at $x = -0.87$ mm and $x = 0.87$ mm are stable positions for particles, as the effect of the ARF performs like an acoustic trap; while the second zero-value point locating at $x = 0$ is an unstable position for particles because the ARF shows a pushing effect. Figures 4(b1)–4(b3) and 4(c1)–4(c3) exhibit the ARF field distribution and the data along the x axis (at $y = 0$) for frequency of 0.66 MHz at $h = 3$ mm and $h = 6$ mm, respectively. Similar results are sketched as in Figs. 4(a1)–4(a3), and the measured data are in well agreement with the simulated results. Therefore, small particles

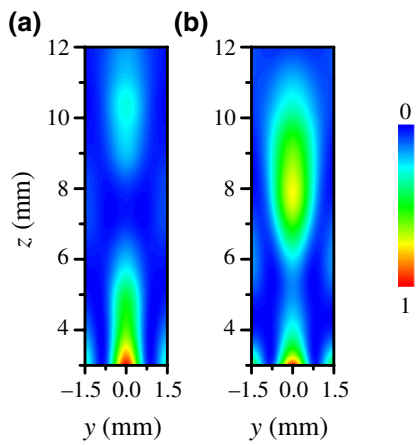


FIG. 3. Simulated intensity field distributions in the y - z plane for frequency of 0.74 MHz (a) and 0.66 MHz (b).

tend to move toward the first and third zero-value points in the generated acoustic field under the action of the ARF and finally stabilize at that position to form a compact ring structure.

III. EXPERIMENTAL SETUP

Next, we give a direct demonstration of particle manipulation with the above acquired subwavelength gradient field. The experimental setup is illustrated in Fig. 5. A piezoelectric transducer is positioned in the bottom of the water tank serving as the generating acoustic source. To get enough ARF, the transducer is connected to a power amplifier (AG 1006) by an impedance matcher (50Ω). The sample is fixed above the source by a specimen holder, and an acoustically transparent thin film placed away from the sample at a certain height is used to support the colored polystyrene microparticles. These motions of the

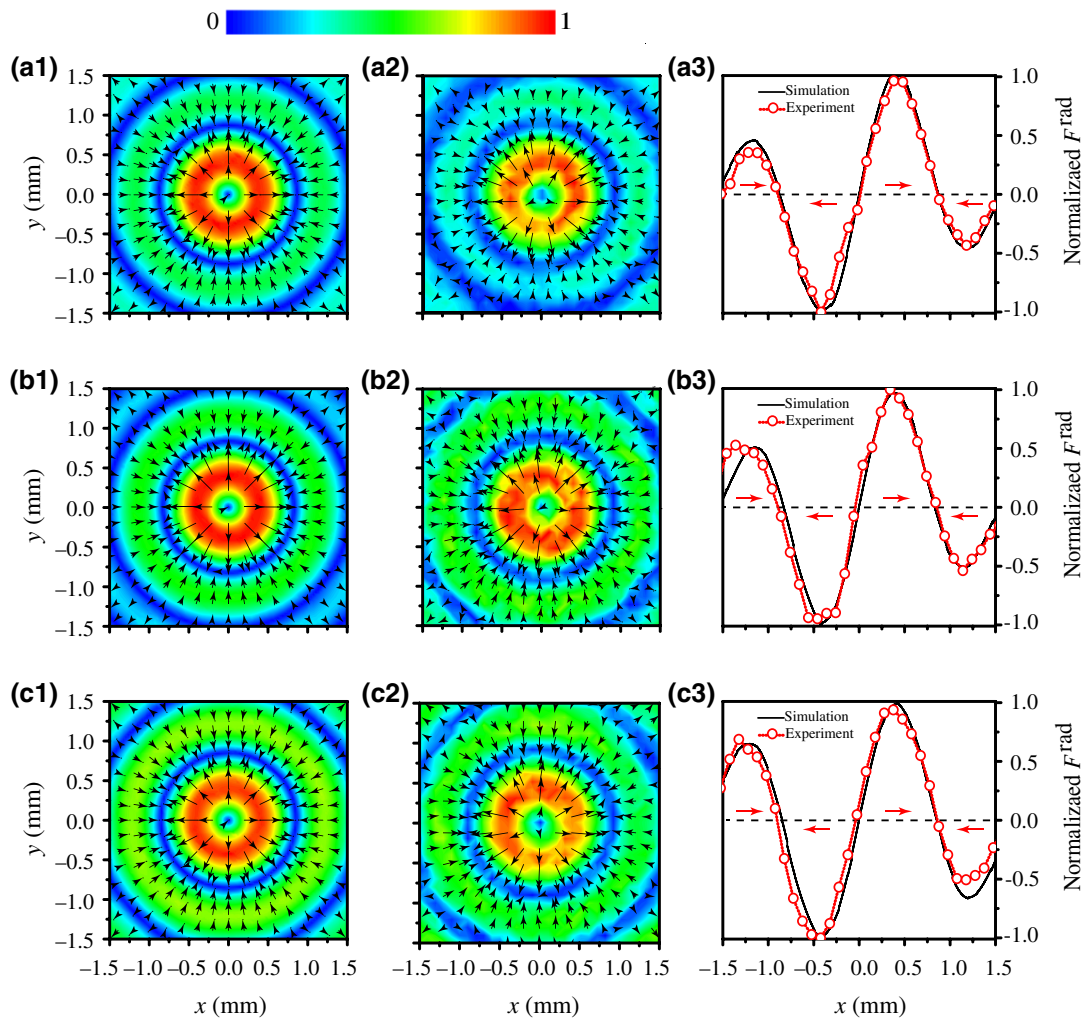


FIG. 4. (a1) and (a2) Simulated and measured ARF distributions in the x - y plane at $h = 3$ mm with the frequency of 0.74 MHz. (a3) The simulated (black solid line) and experimental (red dotted line with circles) ARF distributions along the horizontal line at $y = 0$, the length and orientation of the black arrows represent the magnitude and direction of the ARF, respectively. (b1)–(b3) and (c1)–(c3) are the same as (a1)–(a3), but for the frequency of 0.66 MHz at $h = 3$ mm and $h = 6$ mm, respectively.

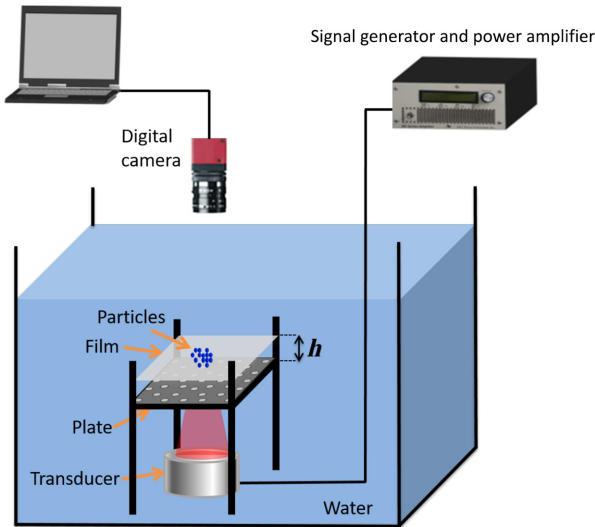


FIG. 5. Schematic of the experimental setup for particle manipulation.

microparticles are recorded by a digital camera mounted on top of the plate.

IV. EXPERIMENTAL RESULTS

A. Pushing manipulation of particles

We perform acoustic manipulation experiment within this small region for two steps: (1) with four particles placed near the center position; (2) with multiparticles placed randomly around the region. The real-time processes of acoustic manipulation on particles for different frequencies of 0.74 and 0.66 MHz at $h = 3$ mm and $h = 6$ mm are recorded (Supplemental Material [43]). Three representative groups of snapshots for the first step are presented in Fig. 6. Initially, four polystyrene particles are randomly placed near the center of the acoustic field in

the thin film [Figs. 6(a1)–6(a3)]. When acoustic waves are normally incident from the bottom of the plate, the four particles are quickly pushed away from the center under the action of the ARF, and finally stabilized [Figs. 6(b1)–6(b3)]. The small blue circles and the big red circles in Fig. 6 label the particles and the stabilized positions of the particles in the gradient acoustic fields, respectively. We predict the stabilized positions according to the acoustic radiation force distribution shown in Fig. 4, which gives the trajectory and locations of the particles in the generated acoustic field. The stabilized positions are the acoustic trap where the directions of acoustic radiation force are opposite away from the trap but both pointing to the trap. The results exhibit the perfect ability of particles pushing of this small subwavelength acoustic field. More details about this process are shown in Movie S1 within the Supplemental Material [43].

B. Trapping manipulation of particles

The second step for particle manipulation further demonstrates the multiparticle trapping process (Fig. 7 and Movie S2 within the Supplemental Material [43]). The operating frequency and the x - y plane spatial position are the same as those selected in the first step. As shown in Figs. 7(a1)–7(a3), a lot of particles with radii of 80–100 μm are randomly distributed in the thin film. When with the acoustic wave incidence, the particles move quickly to the potential well of the gradient field under the action of the ARF, and finally form a ring-shaped structure [Figs. 7(b1)–7(b3)], where the red dashed circles marking the stabilized positions of gradient acoustic fields from Fig. 4. Clearly, this step visually exhibits acoustic manipulation of particle trapping within the small subwavelength region obtained by our simple platform. All the acoustic manipulation experiments definitely confirm our theoretical anticipations.

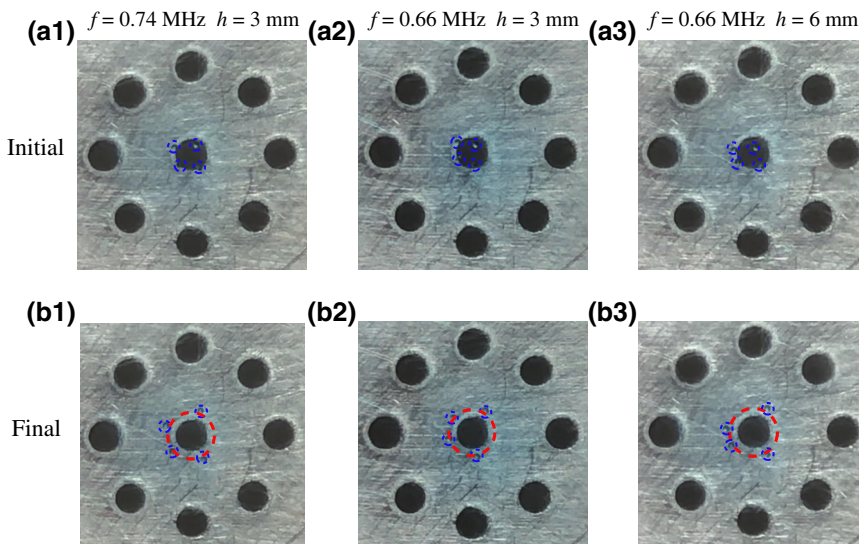


FIG. 6. Snapshots of acoustic pushing of four polystyrene particles with this structure plate. Figures (a1)–(a3), (b1)–(b3) indicate the initial and the final status of particles without and with acoustic wave incidence, where the small blue circles label the particles and the big red circles mark the stabilized positions of gradient acoustic fields from Fig. 4.

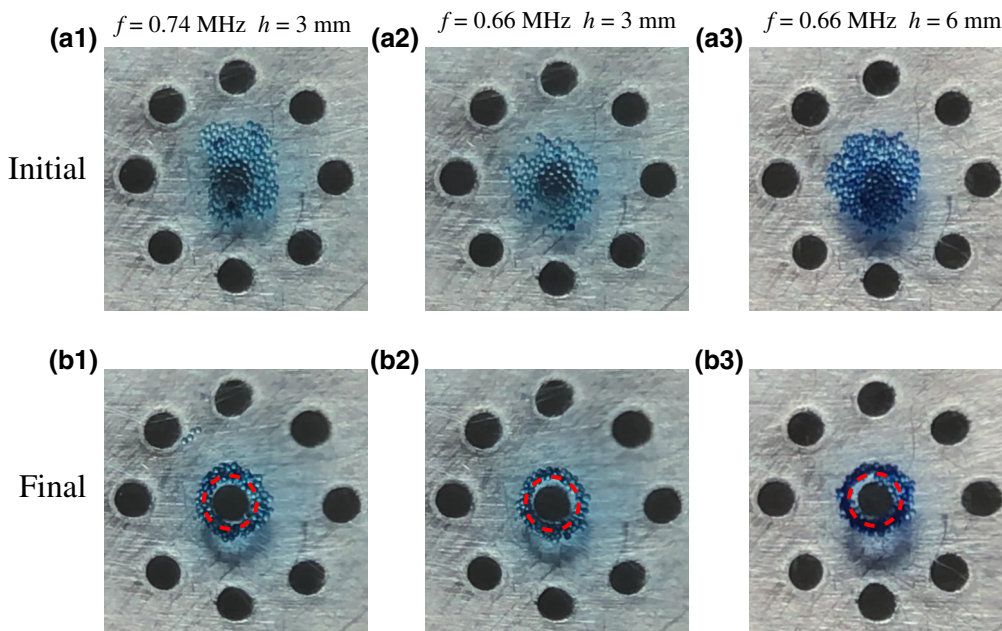


FIG. 7. Snapshots of acoustic trapping of polystyrene particles assisted by the structure plate. Figures (a1)–(a3), (b1)–(b3) indicate the initial and the final status of particles without and with acoustic wave incidence, where the red dashed circles mark the stabilized positions of gradient acoustic fields from Fig. 4.

V. CONCLUSION

In conclusion, by fabricating a structure plate with an eightfold quasiperiodic hole array, we have realized a gradient acoustic field in a small subwavelength region, which still ensures ARF on small particles at different spatial positions for a wide frequency range. The ARF effect of the generated gradient field is numerical and experimental explored, which determines the trajectory and locations of the particles. We further demonstrate acoustic manipulation of flexible pushing and trapping effect on tiny particles within this subwavelength region. We expect this simple platform will bring greater possibilities for multifunctional acoustic manipulation on small particles in biology and medicine.

ACKNOWLEDGMENTS

This work is supported by the National Natural Science Foundation of China (Grants No. 11890701, No. 11974262, and No. 11774275).

- [1] A. M. Seddon, S. J. Richardson, K. Rastogi, T. S. Plivelic, A. M. Squires, and C. Pfrang, Control of nanomaterial self-assembly in ultrasonically levitated droplets, *J. Phys. Chem. Lett.* **7**, 1341 (2016).
- [2] D. Ahmed, A. Ozcelik, N. Bojanala, N. Nama, A. Upadhyay, Y. Chen, W. Hanna-Rose, and T. J. Huang, Rotational manipulation of single cells and organisms using acoustic waves, *Nat. Commun.* **7**, 11085 (2016).
- [3] M. Wu, C. Chen, Z. Wang, H. Bachman, Y. Ouyang, P. Huang, Y. Sadovsky, and T. J. Huang, Separating extracellular vesicles and lipoproteins via acoustofluidics, *Lab Chip* **19**, 1174 (2019).
- [4] A. Ozcelik, J. Rufo, F. Guo, Y. Gu, P. Li, J. Lata, and T. J. Huang, Acoustic tweezers for the life sciences, *Nat. Methods* **15**, 1021 (2018).
- [5] B. Kang, J. Shin, H. Park, C. Rhyou, D. Kang, S. Lee, Y. Yoon, S. Cho, and H. Lee, High-resolution acoustophoretic 3D cell patterning to construct functional collateral cylindroids for ischemia therapy, *Nat. Commun.* **9**, 5402 (2018).
- [6] G. Sitters, D. Kamsma, G. Thalhammer, M. Ritsch-Marte, E. J. G. Peterman, and G. J. L. Wuite, Acoustic force spectroscopy, *Nat. Methods* **12**, 47 (2015).
- [7] Z. Gong and M. Baudoin, Three-Dimensional Trapping and Dynamic Axial Manipulation with Frequency-Tuned Spiraling Acoustical Tweezers: A Theoretical Study, *Phys. Rev. Appl.* **16**, 024034 (2021).
- [8] X. Fan and L. Zhang, Trapping Force of Acoustical Bessel Beams on a Sphere and Stable Tractor Beams, *Phys. Rev. Appl.* **11**, 014055 (2019).
- [9] F. Cai, Z. He, Z. Liu, L. Meng, X. Cheng, and H. Zheng, Acoustic trapping of particle by a periodically structured stiff plate, *Appl. Phys. Lett.* **99**, 253505 (2011).
- [10] Q. Wang, A. Riaud, J. Zhou, Z. Gong, and M. Baudoin, Acoustic Radiation Force on Small Spheres Due to Transient Acoustic Fields, *Phys. Rev. Appl.* **15**, 044034 (2021).
- [11] X. Ren, Q. Zhou, Z. Xu, and X. Liu, Particle Trapping in Arbitrary Trajectories Using First-Order Bessel-Like Acoustic Beams, *Phys. Rev. Appl.* **15**, 054041 (2021).
- [12] M. Baudoin, J. Thomas, R. A. Sahely, J. Gerbedoen, Z. Gong, A. Sivery, O. B. Matar, N. Smagin, P. Favreau, and A. Vlandas, Spatially selective manipulation of cells with single-beam acoustical tweezers, *Nat. Commun.* **11**, 4244 (2020).
- [13] R. Lirette, J. Mobley, and L. Zhang, Ultrasonic Extraction and Manipulation of Droplets From a Liquid-Liquid Interface with Near-Field Acoustic Tweezers, *Phys. Rev. Appl.* **12**, 061001 (2019).

- [14] G. Xu, J. Huang, Y. Zhang, L. Xie, Z. Ni, C. Huang, G. Yao, J. Tu, X. Guo, and D. Zhang, Fourier Acoustical Tweezers: Synthesizing Arbitrary Radiation Force Using Nonmonochromatic Waves on Discrete-Frequency Basis, *Phys. Rev. Appl.* **15**, 044037 (2021).
- [15] A. Franklin, A. Marzo, R. Malkin, and B. W. Drinkwater, Three-dimensional ultrasonic trapping of micro-particles in water with a simple and compact two-element transducer, *Appl. Phys. Lett.* **111**, 094101 (2017).
- [16] D. Baresch, J. Thomas, and R. Marchiano, Observation of a Single-Beam Gradient Force Acoustical Trap for Elastic Particles: Acoustical Tweezers, *Phys. Rev. Lett.* **116**, 024301 (2016).
- [17] J. Lee, S. Teh, A. Lee, H. H. Kim, C. Lee, and K. K. Shung, Single beam acoustic trapping, *Appl. Phys. Lett.* **95**, 073701 (2009).
- [18] J. Wu, Acoustical tweezers, *J. Acoust. Soc. Am.* **89**, 2140 (1991).
- [19] H. Li, Y. Wang, M. Ke, S. Peng, F. Liu, C. Qiu, and Z. Liu, Acoustic manipulating of capsule-shaped particle assisted by phononic crystal plate, *Appl. Phys. Lett.* **112**, 223501 (2018).
- [20] Y. Jia, D. Wu, J. Yao, Q. Wei, Z. Xu, and X. Liu, Acoustic tweezing for both Rayleigh and Mie particles based on acoustic focused petal beams, *Appl. Phys. Lett.* **116**, 263504 (2020).
- [21] F. Li, F. Cai, L. Zhang, Z. Liu, F. li, L. Meng, J. Wu, J. Li, X. Zhang, and H. Zheng, Phononic-Crystal-Enabled Dynamic Manipulation of Microparticles and Cells in an Acoustofluidic Channel, *Phys. Rev. Appl.* **13**, 044077 (2020).
- [22] G. Memoli, M. Calcap, M. Asakawa, D. R. Sahoo, B. W. Drinkwater, and S. Subramanian, Metamaterial bricks and quantization of meta-surfaces, *Nat. Commun.* **8**, 14608 (2017).
- [23] A. Dolev, S. Davis, and I. Bucher, Noncontact Dynamic Oscillations of Acoustically Levitated Particles by Parametric Excitation, *Phys. Rev. Appl.* **12**, 034031 (2019).
- [24] M. A. B. Andrade, A. Marzo, and J. C. Adamowski, Acoustic levitation in mid-air: Recent advances, challenges, and future perspectives, *Appl. Phys. Lett.* **116**, 250501 (2020).
- [25] D. Zang, K. Lin, L. Li, Z. Chen, X. Li, and X. Geng, Acoustic levitation of soap bubbles in air: Beyond the half-wavelength limit of sound, *Appl. Phys. Lett.* **110**, 121602 (2017).
- [26] M. A. B. Andrade, A. L. Bernassau, and J. C. Adamowski, Acoustic levitation of a large solid sphere, *Appl. Phys. Lett.* **109**, 044101 (2016).
- [27] A. Marzo, S. A. Seah, B. W. Drinkwater, D. R. Sahoo, B. Long, and S. Subramanian, Holographic acoustic elements for manipulation of levitated objects, *Nat. Commun.* **6**, 8661 (2015).
- [28] W. J. Xie, C. D. Cao, Y. J. Lü, Z. Y. Hong, and B. Wei, Acoustic method for levitation of small living animals, *Appl. Phys. Lett.* **89**, 214102 (2006).
- [29] Z. Tian, Z. Wang, P. Zhang, T. D. Naquin, J. Mai, Y. Wu, S. Yang, Y. Gu, H. Bachman, Y. Liang, Z. Yu, and T. J. Huang, Generating multifunctional acoustic tweezers in petri dishes for contactless, precise manipulation of bioparticles, *Sci. Adv.* **6**, eabb0494 (2020).
- [30] G. T. Silva, J. H. Lopes, J. P. Leão-Neto, M. K. Nichols, and B. W. Drinkwater, Particle Patterning by Ultrasonic Standing Waves in a Rectangular Cavity, *Phys. Rev. Appl.* **11**, 054044 (2019).
- [31] L. Tian, N. Martin, P. G. Bassindale, A. J. Patil, M. Li, A. Barnes, B. W. Drinkwater, and S. Mann, Spontaneous assembly of chemically encoded two-dimensional coacervate droplet arrays by acoustic wave patterning, *Nat. Commun.* **7**, 13068 (2016).
- [32] Y. Gu, C. Chen, J. Rufo, C. Shen, Z. Wang, P. Huang, H. Fu, P. Zhang, S. A. Cummer, Z. Tian, and T. J. Huang, Acoustofluidic holography for micro-to nanoscale particle manipulation, *ACS Nano* **14**, 14635 (2020).
- [33] T. Wang, M. Ke, S. Xu, J. Feng, C. Qiu, and Z. Liu, Dexterous acoustic trapping and patterning of particles assisted by phononic crystal plate, *Appl. Phys. Lett.* **106**, 163504 (2015).
- [34] L. Meng, X. Cui, C. Dong, X. Liu, W. Zhou, W. Zhang, X. Wang, L. Niu, F. Li, F. Cai, J. Wu, and H. Zheng, Microbubble enhanced acoustic tweezers for size-independent cell sorting, *Appl. Phys. Lett.* **116**, 073701 (2020).
- [35] K. Wang, W. Zhou, Z. Lin, F. Cai, F. Li, J. Wu, L. Meng, L. Niu, and H. Zheng, Sorting of tumour cells in a microfluidic device by multi-stage surface acoustic waves, *Sens. Actuators, B* **258**, 1174 (2018).
- [36] F. Li, F. Cai, Z. Liu, L. Meng, M. Qian, C. Wang, Q. Cheng, M. Qian, X. Liu, J. Wu, J. Li, and H. Zheng, Phononic-Crystal-Based Acoustic Sieve for Tunable Manipulations of Particles by a Highly Localized Radiation Force, *Phys. Rev. Appl.* **1**, 051001 (2014).
- [37] P. Gires and C. Poulain, Near-field acoustic manipulation in a confined evanescent Bessel beam, *Commun. Phys.* **2**, 94 (2019).
- [38] Q. Lin, W. Zhou, F. Cai, F. Li, X. Xia, J. Wang, D. Zhao, F. Yan, L. Meng, and H. Zheng, Trapping of sub-wavelength microparticles and cells in resonant cylindrical shells, *Appl. Phys. Lett.* **117**, 053501 (2020).
- [39] Y. Shen, Y. Peng, F. Cai, K. Huang, D. Zhao, C. Qiu, H. Zheng, and X. Zhu, Ultrasonic super-oscillation wavepackets with an acoustic meta-lens, *Nat. Commun.* **10**, 3411 (2019).
- [40] M. Ke, Z. He, S. Peng, Z. Liu, and J. Shi, Surface Resonant-States-Enhanced Acoustic Wave Tunneling in Two-Dimensional Phononic Crystals, *Phys. Rev. Lett.* **99**, 044301 (2007).
- [41] Y. Ye, M. Ke, C. Li, T. Wang, C. Qiu, and Z. Liu, Acoustic lens: A thin plate with quasi-periodic array of holes, *Solid State Commun.* **185**, 35 (2014).
- [42] L. P. Gor'kov, On the forces acting on a small particle in an acoustical field in an ideal fluid, *Sov. Phys. - Dokl.* **6**, 773 (1962).
- [43] See Supplemental Material at <http://link.aps.org/supplemental/10.1103/PhysRevApplied.17.014026> for movies about the detailed experimental process.